Desalination and Water Treatment
www.deswater.com
doi: 10.1080/19443994.2014.922441

55 (2015) 1018–1025
July

Taylor & Francis
Taylor & Francis Group

Efficient degradation of methylene blue by magnetically separable Fe_3O_4/chitosan/TiO_2 nanocomposites

Ying Xiang[a,b], Hui Wang[a,b], Yu He[a,b,*], Gongwu Song[a,b,*]

[a]*Hubei Collaborative Innovation Center for Advanced Organic Chemical Materials, College of Chemistry and Chemical Engineering, Hubei University, Wuhan 430062, China, Tel. +86 2788662747; emails: 772926945@qq.com (Y. Xiang), 431605627@qq.com (H. Wang), heyu@hubu.edu.cn (Y. He), songgw@hubu.edu.cn (G. Song)*
[b]*Ministry-of-Education Key Laboratory for the Synthesis and Application of Organic Functional Molecules, College of Chemistry and Chemical Engineering, Hubei University, Wuhan 430062, China*

Received 25 October 2013; Accepted 1 May 2014

ABSTRACT

In this work, a facile and low-cost method for fabrication of the Fe_3O_4/chitosan/TiO_2 nanocomposites with good adsorptive, photocatalytic, regenerated, and magnetic properties was demonstrated. The synthesized nanocomposites had potential applications for adsorption and degradation of organic pollutants in wastewater. Under the optimal condition, degradation rate of methyl blue by the Fe_3O_4/chitosan/TiO_2 nanocomposites was 93%. The renewable photocatalytic activity of the nanocomposites was also investigated. After multi-run experiments, the reused Fe_3O_4/chitosan/TiO_2 nanocomposites still kept high photocatalytic performance. Thus, Fe_3O_4/chitosan/TiO_2 nanocomposites could serve as convenient, effective, and recyclable photocatalysts.

Keywords: Fe_3O_4/chitosan/TiO_2 nanocomposites; Magnetic property; Photocatalysis; Regeneration

1. Introduction

Nano-TiO_2 is a highly active photocatalyst with favorable properties including low cost, stability, and non-toxicity [1–11]. This photocatalytic process by nano-TiO_2 can decompose almost all the organic pollutants in water under moderate conditions, which is facile, economical, and environmental friendly [1–11]. Nevertheless, nano-TiO_2 also encounters great difficulties to be separated and recycled after the wastewater treatment. Moreover, the nano-TiO_2 has a strong tendency to agglomerate which will decrease the photocatalytic activity [12–14]. In order to overcome the disadvantages of the nano-TiO_2, several methods have been developed to load TiO_2 on different support [12–14]. Despite the fact that significant progress has been made in the development of nano-TiO_2-based nanocomposites as the photocatalyst, it is still a challenge to explore novel and easy-recycled nano-TiO_2-based photocatalyst for inexpensive, facile, and non-toxic wastewater treatment.

Chitosan (CTS) is one of the most important adsorbents with high capacity for the adsorption of metal ions and dyes, which has been widely used in wastewater treatment [15–18]. The adsorption capability of dyes in wastewater by chitosan is reported at 1,000–1,100 g kg^{-1} [19], which is several times larger than activated carbon, because the amino (–NH_2) and

*Corresponding author.

hydroxy (–OH) groups of CTS chains can coordinate and react with contaminants [20,21]. Although CTS have the potential applications in wastewater treatment [21–26], it cannot be separated and regenerated from the wastewater. Thus, to produce the nanocomposites with both the photocatalytic ability of nano-TiO_2 and the adsorption capacity of the CTS will do favor to the removal of adsorbed contaminants and the regeneration of the CTS.

Herein, we constructed a novel Fe_3O_4/CTS/TiO_2 nanocomposite for the cost-effective, facile, sensitive, and non-toxic treatment of wastewater (Fig. 1). The addition of magnetic Fe_3O_4 nanoparticles made the nanocomposites separated from the water by an external magnetic field [27,28]. Compared with the conventional photocatalytic materials, Fe_3O_4/CTS/TiO_2 nanocomposites not only gave high efficiency in photocatalysis, but also provided excellent magnetic and adsorption properties, which made the nanocomposite easy-recycled and regenerated. Owing to above merits, Fe_3O_4/CTS/TiO_2 nanocomposites could serve as convenient, effective, and recyclable photocatalysts.

2. Experimental section

2.1. Reagents

All the used reagents were of analytical grade. P-25 TiO_2, chitosan, glacial acetic acid, Span-80, liquid paraffin, and glutaraldehyde (25%) were purchased from Degussa Co. (Nanning, China), Qingdao Yunzhou Biological Reagent Co. (Qingdao, China), Tianjin Tianli Chemical Reagent Co. (Tianjin, China), Tianjin Guangcheng Chemical Reagent Co. (Tianjin, China), Tianjin Bodi Chemical Industry Co. (Tianjin, China), Shanghai Chemical Reagent Co. (Shanghai, China). The concentration of methylene blue (MB) stock solution was 50 mM. NaOH and H_2SO_4 were used to adjust pH of the reaction solution. Doubly distilled water was obtained from water purification system (Chongqing Lidi Modern Water Technical Equipment Co.).

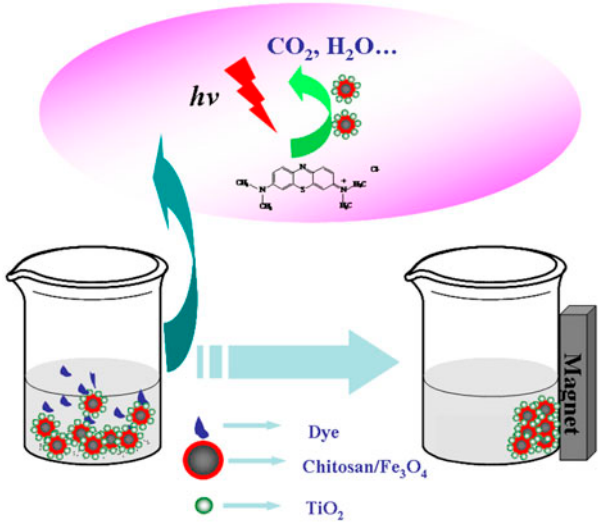

Fig. 1. Schematic diagram of the nanocomposites for photocatalysis of methylene blue.

2.2. Apparatus

The crystalline structure and composition of the Fe_3O_4/CTS/TiO_2 were identified, respectively, by a D/max-IIIC X-ray diffractometer (Shimadzu, Japan). The morphologies of the prepared samples were examined using JEM-100SX electron microscope (Nicolet, Japan). Fourier transform infrared (FTIR) spectra were taken with a Spectrum One FTIR spectrophotometer (Perkin–Elmer, America) at room temperature. Element analysis was performed with optimal 8,000 inductively coupled plasma mass spectrometer (ICPMS) (Perkin–Elmer, America). The UV–vis absorption measurements were performed on ZF-I Three-operating UV analyzer (Gucun Electricity Light Instrumental Factory, China). AWH-2 vortex mixer (Huxi Instrumental Co., China) was used to blend the solution. A pHB-4 pH meter (Ruosull Technology Co., China) was used to measure the pH of the solution. Photocatalytic oxidation of the organic compounds occurred under the illumination of the UV lamp (8 W, Feiyang Instrumental Co., China).

2.3. The synthesis of Fe_3O_4 magnetic nanoparticles

Fe_3O_4 nanoparticles were synthesized through the solvents thermal reduction of $FeCl_3$ [26]. About 0.54 g $FeCl_3$, 1.8 g sodium acetate, and 0.5 g polyether imide were dissolved in 20 ml glycol and kept stirring for 1 h to obtain deep yellowish brown stickiness liquid. The mixture was sealed in a Teflon-lined stainless-steel autoclave (25 ml). The autoclave was heated to and maintained at 200℃ for 12 h. After the reaction, the black products were washed several times with ethanol and dried at 60℃ for 6 h.

2.4. The preparation of Fe_3O_4/CTS carrier

The 400 mg CTS and 400 mg Fe_3O_4 nanoparticles were dissolved in 20 ml 3% acetic acid to form a mixture solution. The above solution was dropped slowly to the three-necked flask containing 4 ml Span-80 and 80 ml liquid paraffin and stirred for 30 min at room temperature. Then, 1.0 ml 25% glutaraldehyde was

added and reacted for 1 h at 40℃. The temperature was increased to 65℃ and kept reacting for 3 h. The products were washed with anhydrous ether, acetone, and water successively. Finally, the products were separated by magnet and dried at 60℃.

2.5. The synthesis of Fe_3O_4/CTS/TiO_2 nanocomposites

The synthesis of Fe_3O_4/CTS/TiO_2 nanocomposites was based on a previous publication with minor modification [30]. The powder of P25 TiO_2 was calcined at 400℃ for 1 h before reaction. One gram TiO_2 and 1 g Fe_3O_4/CTS nanoparticles were mixed in 100 ml doubly distilled water, then diacetylmethane and OP-10 were added as dispersant and emulsifier, respectively. The nanocomposites were obtained through magnetic separation and dried at 60℃.

2.6. Photocatalytic activity measurement

The photocatalytic activity of the Fe_3O_4/CTS/TiO_2 nanocomposites was evaluated by the degradation of MB. The solution was irradiated by a UV lamp. At a given irradiation time interval (10 min), 3 ml aliquots was collected. The absorbance of solution at 664 nm was monitored to determine the concentration of MB. The degradation rate of the MB was evaluated by the equation: $(D) = [(A_0 - A)/A_0] \times 100\% = [(C_0 - C)/C_0] \times 100\%$, where A and A_0 were the absorbance of MB solution after degradation and before degradation, C and C_0 were the concentration of MB after and before degradation.

3. Results and discussion

3.1. Preparation and characterization of Fe_3O_4/CTS/TiO_2 nanocomposites

Fe_3O_4 nanoparticles were synthesized via modified solvent thermal method [29]. Fig. 2(a) shows the transmission electron microscope (TEM) image of Fe_3O_4 nanoparticles. From the TEM image, Fe_3O_4 nanoparticles were spherical with a particle size of about 50 nm (Fig. 2(a)). Magnetic measurements of Fe_3O_4 nanoparticles were investigated with a vibrating sample magnetometer (VSM). The hysteresis loop of Fe_3O_4 nanoparticles is shown in Fig. 2(b) and (c). The Fe_3O_4 nanoparticles showed ferromagnetic behavior with magnetic saturation value of 57 emu/g. The Fe_3O_4 nanoparticles could help in the separation of the Fe_3O_4/CTS/TiO_2 nanocomposites from the water under an external magnetic field after the wastewater treatment.

The synthesis of Fe_3O_4/CTS/TiO_2 nanocomposites was carried out on the basis of the reaction of Fe_3O_4-chitosan, P-25 TiO_2, diacetylmethane, and OP-10 according to previously reported procedure [30]. The acquired nanocomposites were characterized by XRD (Fig. 3(a)), FTIR (Fig. 2(b)), UV–vis spectra (Fig. 3(c)), TEM (Figs. 3(d), (e), and 2(f)) and magnetic measurements (Fig. 4). Fig. 3(a) displays the XRD pattern of TiO_2 nanoparticles (Fig. 3(a), curve 1) and Fe_3O_4/CTS/TiO_2 nanocomposites (Fig. 3(a), curve 2). The diffraction peak of pure TiO_2 anatase appeared at 25.2°. After forming the Fe_3O_4/CTS/TiO_2 nanocomposites, the diffraction peaks corresponding to typical TiO_2 at 25.2° were still observed, indicating that the Fe_3O_4/CTS/TiO_2 nanocomposites prepared here was mainly composed of anatase phase. Six characteristic peaks ($2\theta = 29.91°$, 35.36°, 43.02°, 53.33°, 56.98°, and 62.48°) of curve 2 in Fig. 3(a) marked by their Miller indices ((2 2 0), (3 1 1), (4 0 0), (4 2 2), (5 1 1), and (4 4 0)) were observed in the case of Fe_3O_4 nanoparticles, respectively. Fig. 3(b) shows the FTIR spectra of pure TiO_2 nanoparticles (Fig. 3(b), curve 1), Fe_3O_4/CTS (Fig. 3(b), curve 2) and Fe_3O_4/CTS/TiO_2 nanocomposites (Fig. 3(b), curve 3). The typical bands assigned to the Fe–O stretching were visible at around 599 cm^{-1} (curve 2). The bands at 1,079 and 3,466 cm^{-1} were ascribed to the C–H vibration and O–H vibration, respectively. In addition, the band at 1,378 and 1,651 cm^{-1} was assigned to amide I and amide III of chitosan (curve 2). In the curve of Fe_3O_4/CTS/TiO_2 nanocomposites (curve 3), owing to the covalent interaction between TiO_2 nanoparticles and the surface of Fe_3O_4/CTS nanoparticles, the characteristic peak of 762 cm^{-1} (Ti–O expansion) shift to 709.65 cm^{-1} in the FTIR spectra [31], and the characteristic peak of chitosan at 1,651 and 1,378 cm^{-1} shift to 1510.94 and 1345.24 cm^{-1}, respectively. According to XRD and FTIR, the TiO_2 nanoparticles are load on the surface of the Fe_3O_4/CTS nanoparticles.

The UV–vis spectra were recorded for the samples of TiO_2, TiO_2/CTS and Fe_3O_4/CTS/TiO_2 in Fig. 3(c). The modification of CTS on the surface of TiO_2 had no influence on the UV–vis curve of TiO_2 nanoparticles. The complex of Fe_3O_4 nanoparticles to TiO_2 nanoparticles led to a shift of the absorption edge toward longer wavelengths, indicating a decrease in the band gap energy and more photogenerated electrons and holes could participate in the photocatalytic reactions. This alteration could force TiO_2 to be activated in the visible region.

Fig. 3(d), (e), and (f) display the TEM images of pure TiO_2 nanoparticles, Fe_3O_4/CTS nanoparticles, and Fe_3O_4/CTS/TiO_2 nanocomposites. The diameter of TiO_2 nanoparticles was 20 nm (Fig. 3(d)).

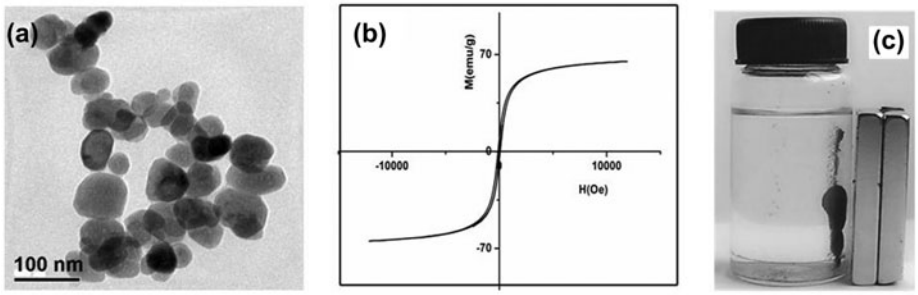

Fig. 2. (a) TEM images of Fe_3O_4 nanoparticles. (b) Magnetic properties of Fe_3O_4 nanoparticles. (c) Demonstration of magnetic separation of Fe_3O_4 nanoparticles in water by a magnet.

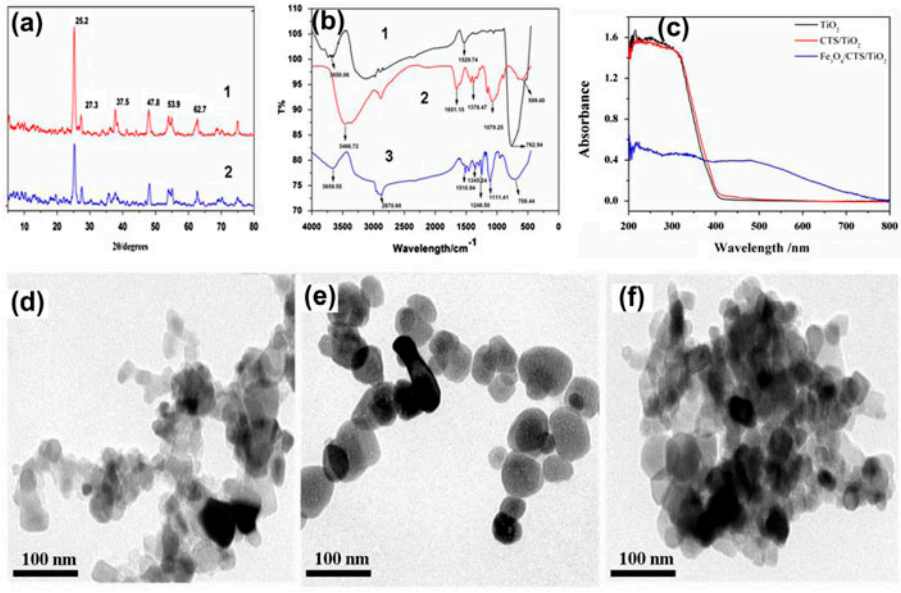

Fig. 3. (a) XRD diffraction patterns of TiO_2 nanoparticles (1) and Fe_3O_4/CTS/TiO_2 nanocomposites (2); (b) FTIR spectra of pure TiO_2 nanoparticles (1), Fe_3O_4/CTS (2), and Fe_3O_4/CTS/TiO_2 nanocomposites (3); (c) The UV–vis spectra was recorded for the samples of TiO_2, TiO_2/chitosan and Fe_3O_4/chitosan/TiO_2; (d) TEM images of pure TiO_2 nanoparticles; (e) TEM images of Fe_3O_4/CTS nanoparticles; and (f) TEM images of Fe_3O_4/CTS/TiO_2 nanocomposites.

The TEM of Fe_3O_4/CTS/TiO_2 nanocomposites showed that the TiO_2 nanoparticles were covered on surface of the Fe_3O_4/CTS nanoparticles, indicating the formation of nanocomposites (Fig. 3(f)). Elemental analysis was used to identify the composition of the Fe_3O_4/CTS/TiO_2 nanocomposites. Based on the ICP analysis, the content of the Fe and Ti was 13.6 and 31.4%, respectively. The BET surface areas of TiO_2 nanoparticles, Chitosan-TiO_2 nanoparticles, and Fe_3O_4/CTS/TiO_2 nanocomposites were measured. The S_{BET} values were 42, 62, and 61 m^2/g for TiO_2 nanoparticles, TiO_2/CTS nanoparticles, and Fe_3O_4/CTS/TiO_2, respectively. We investigate the magnetic properties of as-synthesized Fe_3O_4/CTS/TiO_2 nanocomposites. The modification of chitosan on the surface of Fe_3O_4 nanoparticles nearly had no influence on the magnetic properties of as-synthesized Fe_3O_4 nanoparticles. The magnetization saturation value of Fe_3O_4/CTS/TiO_2 nanocomposites was 4.2 emu g^{-1}, which verifies that the Fe_3O_4/Chitosan/TiO_2 nanocomposites can be separated by an external applied magnetic field (Fig. 4).

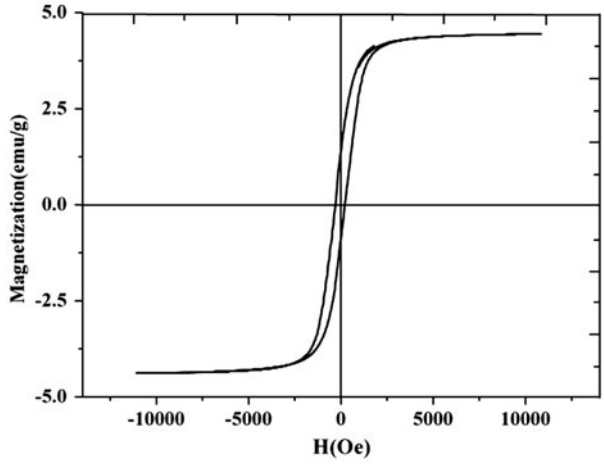

Fig. 4. The VSM picture of $Fe_3O_4/CTS/TiO_2$ nanocomposites.

3.2. Effect of dosage of $Fe_3O_4/CTS/TiO_2$ nanocomposites

The photocatalytic activity of $Fe_3O_4/CTS/TiO_2$ nanocomposites was demonstrated by a photocatalytic degradation of MB in water. The concentration of methylene blue via absorbance exhibited good linear correlations. Then, we evaluated the factors influenced on the photocatalytic reaction such as the dosage of the $Fe_3O_4/CTS/TiO_2$ nanocomposites, the pH value, and the illumination time. Fig. 5(a) shows the degradation ratio of MB with various $Fe_3O_4/CTS/TiO_2$ nanocomposite dosages. The degradation ratio of MB increased when the concentration of nanocomposites was from 0.5 to $1\,g\,L^{-1}$, and then leveled off with the further increased concentration of $Fe_3O_4/CTS/TiO_2$ nanocomposites. The reason for this phenomenon was that higher dosages decreased the penetration of light and thus reduced the efficiency of the photocatalytic oxidation. Therefore, $1\,g\,L^{-1}$ $Fe_3O_4/CTS/TiO_2$ nanocomposites were chosen for the further experiments.

3.3 Effect of pH on the photocatalytic degradation

The pH of aquatic environment played an important role on the photocatalytic degradation of organic contaminants. In Fig. 5(b), the photodegradation ratio increased with the increase of pH value , and then declined when the pH was rising to 6.9 due to the isoelectric point of TiO_2 with the pH 6.9 [32]. Because the pH of conventional wastewater was usually lower than 7.0, pH 5.5 was chosen.

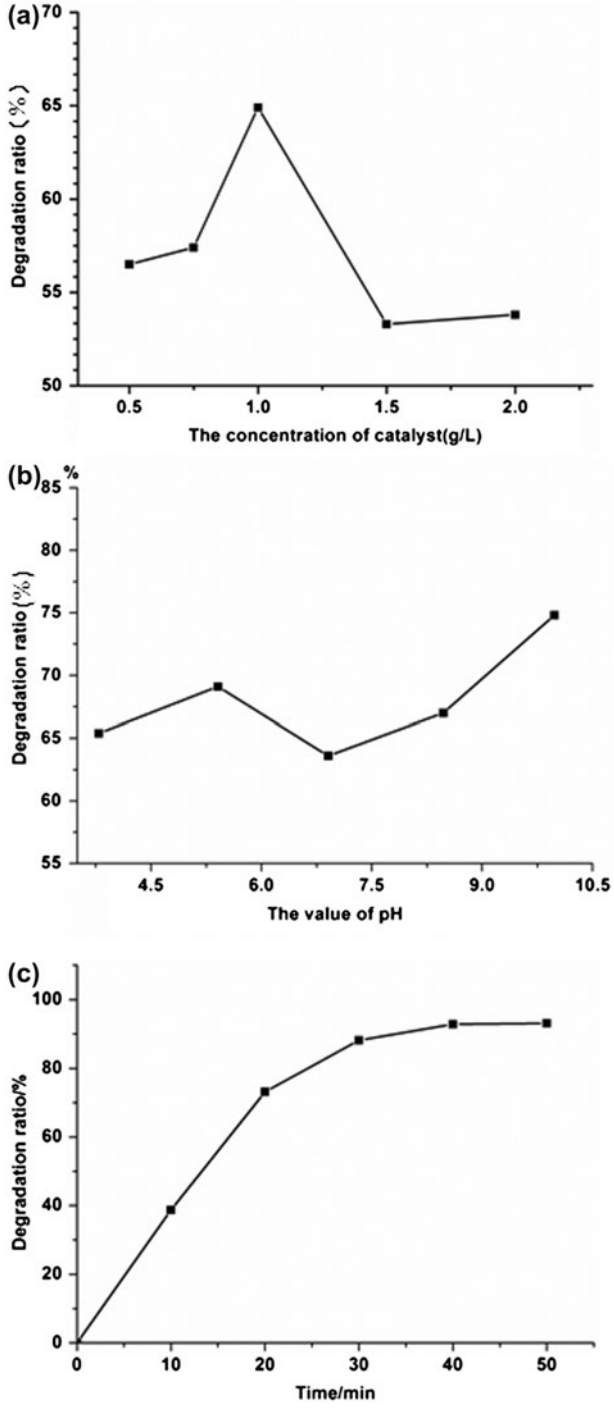

Fig. 5. (a) Effect of the dosage of $Fe_3O_4/CTS/TiO_2$ nanocomposites on the photocatalytic ability. The concentration of MB is 4×10^{-6} mol l. (b) Effect of value of pH on the photocatalytic ability. The concentration of MB and $Fe_3O_4/CTS/TiO_2$ nanocomposites are $4\times10^{-6}\,mol\,l^{-1}$ and $1\,g\,l^{-1}$, respectively. (c) Effect of the illumination time on the photocatalytic degradation of MB. The concentrations of MB and $Fe_3O_4/CTS/TiO_2$ nanocomposites are $4\times10^{-6}\,mol\,l^{-1}$ and $1\,g\,l^{-1}$, respectively.

3.4. Comparison of influence of the illumination time

The effect of illumination time of photocatalytic oxidation was investigated and the results are shown in Fig. 5(c). The degradation ratio increased with increment of illumination time, and then approached a stable value after illumination over 30 min. Therefore, 30 min was chosen for the further experiment.

3.5. Comparison of different photocatalysis systems

In Fig. 6, different photocatalytic systems on the degradation of MB were investigated. After 40 min of irradiation with UV light in the presence of 1 g L^{-1} catalyst, the degradation ratio of MB by the Fe_3O_4/CTS/TiO_2 nanocomposites system was increased to 92.8%, which was close to the degradation ratio by using the pure P25 TiO_2 powder. Fe_3O_4/CTS nanoparticles also exhibited the photocatalytic ability to some extent. There were some synergic activities with the combination of adsorption and photodegradation functions of Fe_3O_4/CTS/TiO_2 nanocomposites system. The results indicated that the photocatalytic activity of TiO_2 nanoparticles was not declined after being loaded.

3.6. The mechanism of the photocatalytic system

In order to demonstrate the photocatalytic activity and mechanism for degradation of MB, we investigated the photocatalytic decomposition of MB by UV–vis absorption and FTIR measurements (Fig. 7). In Fig. 7(a), the absorption peaks at 235, 292, 620, and 664 nm correspond to the MB [30]. The two typical absorption peaks at 292 and 664 nm represented the benzene and chromophoric group of MB, respectively. The photocatalytic decomposition of MB by Fe_3O_4/CTS/TiO_2 nanocomposites was very fast, and the MB solution had almost completely decolorized after illumination with UV light for 50 min (Fig. 7(b)). During the reaction process, the characteristic absorption peak at 664 nm decreased dramatically and nearly disappeared after 50 min by photocatalysis, indicating that photocatalysis degradation of MB had resulted in fragmentation of chromophoric group. Fig. 7(c) displays the FTIR spectra of MB before and after photocatalytic degradation. In the sample of MB, the peaks at 1,590,

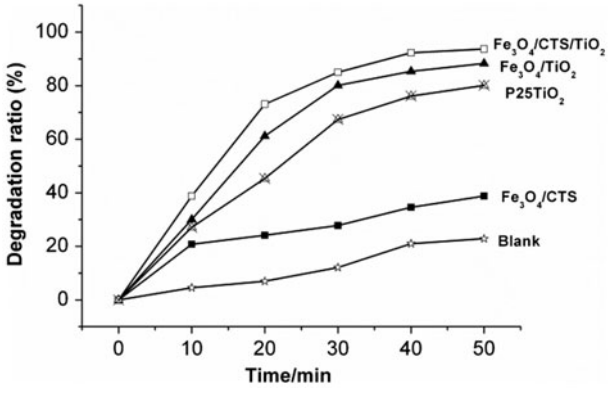

Fig. 6. Effect of the different photocatalytic system for degradation of MB. The concentration of MB is 4 μM. The concentration of P25 TiO_2, Fe_3O_4/CTS/TiO_2 nanocomposites, and Fe_3O_4/CTS are 1 mg ml^{-1}.

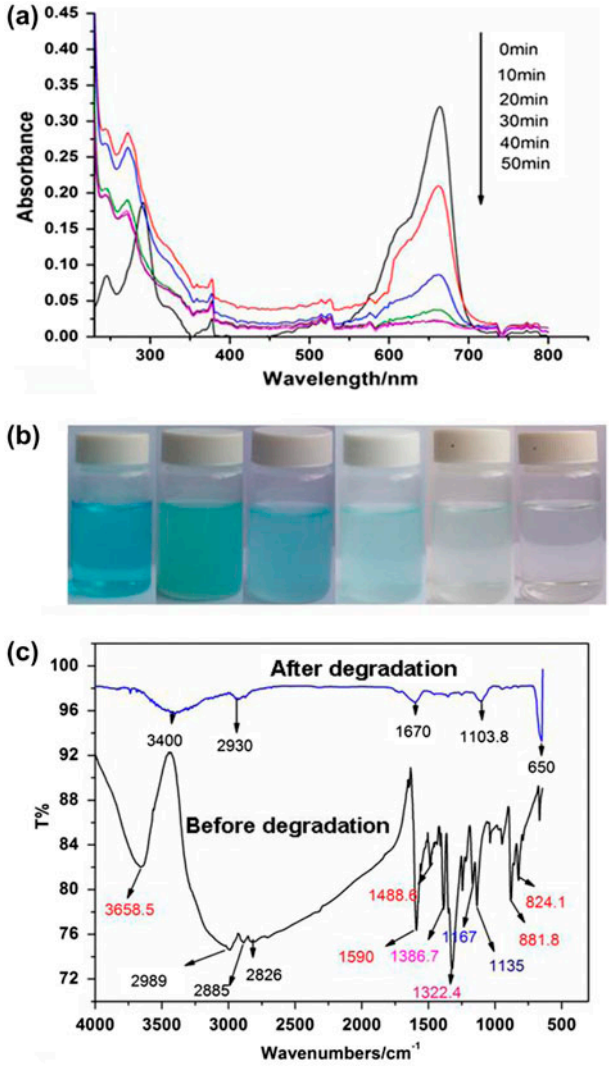

Fig. 7. (a) Absorption spectra of MB solutions in the presence of Fe_3O_4/CTS/TiO_2 nanocomposites under different UV light irradiation time. (b) The color reduction with increase of UV light irradiation time correspondingly. (c) The FTIR spectra of MB and the product after photocatalytic degradation.

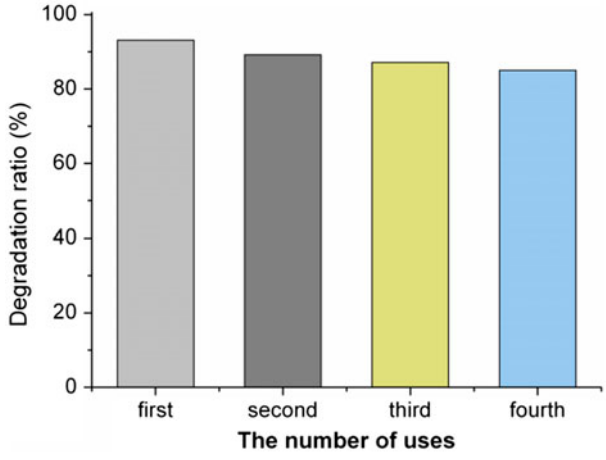

Fig. 8. The durability of the Fe_3O_4/CTS/TiO_2 nanocomposites. The concentration of MB and Fe_3O_4/CTS/TiO_2 nanocomposites are 4.00×10^{-6} mol l^{-1} and 1.00 g l^{-1}, respectively.

1488.6, 881.8, and 824.1 cm^{-1} represented the benzene; the positions at 1135 and 1167 cm^{-1} was vibrating peak of C–H, furthermore, 1386.7 cm^{-1} represented $–CH_3$, and 1322.4 cm^{-1} represented the C–H of double bond. After photocatalytic degradation, the three characteristic absorption peaks including benzene, C–N chromophoric group, and $–CH_3$ band all disappeared. Therefore, the structure of MB was damaged significantly after photocatalytic degradation.

3.7. The durability of the Fe_3O_4/CTS/TiO_2 nanocomposites

The reusability of the recovered Fe_3O_4/CTS/TiO_2 nanocomposites was tested and is shown in Fig. 8. After the multi-run experiments, the photocatalytic ability was slightly deteriorated which showed satisfactory stability of the photocatalytic performance. Although the Fe_3O_4/CTS/TiO_2 nanocomposites may lose some TiO_2 coating from the long-term use, it was possible to restore the used Fe_3O_4/CTS/TiO_2 nanocomposites by repeating the TiO_2-coating process for the recovery of the photoactivity.

4. Conclusion

In summary, a facile method was employed to prepare Fe_3O_4/CTS/TiO_2 nanocomposites with high adsorption capacity and photocatalytic activity. The photocatalytic activity of the nanocomposite under UV irradiation was evaluated by the MB aqueous solution. The Fe_3O_4 nanoparticles could be contributed to the regeneration and separation of Fe_3O_4/CTS/TiO_2 nanocomposites from the water. After recycling the photocatalyst five times for MB photodegradation, the degradation reaction rate constant of the Fe_3O_4/CTS/TiO_2 nanocomposites was stable. This demonstrated that the as-prepared composites could be used as convenient, recyclable photocatalysts.

Acknowledgments

This work was financially supported by the Scientific Research Foundation of Education Commission of Hubei Province (Q20111010 and T201101), the Natural Science Foundation of Hubei Province (2011CDB059 and 2011CDA111), and Research Fund for the Doctoral Program of Higher Education of China (20114208120006).

References

[1] H. Tong, S.X. Ouyang, Y.P. Bi, N. Umezawa, M. Oshikiri, J.H. Ye, Nano-photocatalytic materials: Possibilities and challenges, Adv. Mater. 24 (2012) 229–251.
[2] W. Karran, P. Georgios, S. Wolfgang, Photocatalytic carbon nanotube TiO_2 composites, Adv. Mater. 21 (2009) 2233–2239.
[3] S. Wang, L.X. Yi, J.E. Halpert, X.Y. Lai, Y.Y. Liu, H.B. Cao, R.B. Yu, D. Wang, Y.L. Li, A novel and highly efficient photocatalyst based on P25-graphdiyne nanocomposite, Small 8 (2008) 265–271.
[4] J. Du, X.Y. Lai, N.L. Yang, Hierarchically ordered macro-mesoporous TiO_2-graphene composite films: Improved mass transfer, reduced charge recombination, and their enhanced photocatalytic activities, ACS Nano 5 (2011) 590–596.
[5] Y.F. Li, Z.P. Liu, Particle size, shape and activity for photocatalysis on titania anatase nanoparticles in aqueous surroundings, J. Am. Chem. Soc. 133 (2011) 15743–15752.
[6] H. Wang, S.H. Zhong, Y. He, G.W. Song, Molecular sieve 4A–TiO_2–$K_2Cr_2O_7$ coexisted system as sensor for chemical oxygen demand, Sens. Actuators, B 160 (2011) 189–195.
[7] S. Yurdakal, G. Palmisano, V. Loddo, Nanostructured rutile TiO_2 for selective photocatalytic oxidation of aromatic alcohols to aldehydes in water, J. Am. Chem. Soc. 130 (2008) 1568–1569.
[8] H.X. Li, Z.F. Bian, J. Zhu, Mesoporous Au/TiO_2 nanocomposites with enhanced photocatalytic activity, J. Am. Chem. Soc. 129 (2007) 4538–4539.
[9] M.Y. Abdelaal, R.M. Mohamed, Novel Pd/TiO_2 nanocomposite prepared by modified sol–gel method for photocatalytic degradation of methylene blue dye under visible light irradiation, J. Alloys Compd. 576 (2013) 201–207.
[10] X.J. Bai, R.L. Zong, C.X. Li, D. Liu, Y.F. Liu, Y.F. Zhu, Enhancement of visible photocatalytic activity via Ag@C_3N_4 core–shell plasmonic composite, Appl. Catal., B 147 (2014) 82–91.

[11] T. Harifi, M. Montazer, Photo-, bio-, and magneto-active colored polyester fabric with hydrophobic/hydrophilic and enhanced mechanical properties through synthesis of $TiO_2/Fe_3O_4/Ag$ nanocomposite, Ind. Eng. Chem. Res. 53 (2014) 1119–1129.
[12] Z.Y. Ji, J.S. Yuan, X.G. Li, Removal of ammonium from wastewater using calcium form clinoptilolite, J. Hazard. Mater. 141 (2007) 483–488.
[13] Y. Kim, M. Yoon, TiO_2/Y-zeolite encapsulating intramolecular charge transfer molecules: A new photocatalyst for photoreduction of methyl orange in aqueous medium, J. Mol. Catal. A: Chem. 168 (2001) 257–263.
[14] S. Anandan, M. Yoon, Photocatalytic activities of the nano-sized TiO_2-supported Y-zeolites, J. Photochem. Photobiol. C: Photochem. Rev. 4 (2003) 5–18.
[15] F.C. Wu, R.L. Tseng, R.S. Juang, Comparative adsorption of metal and dye on flake- and bead-types of chitosans prepared from fishery wastes, J. Hazard. Mater. 73 (2000) 63–75.
[16] K.H. Chu, Removal of copper from aqueous solution by chitosan in prawn shell: Adsorption equilibrium and kinetics, J. Hazard. Mater. 90 (2002) 77–95.
[17] W.S. Ngah, A. Kamari, S. Fatinathan, P. W. Ng, Adsorption of chromium from aqueous solution using chitosan beads, Adsorption 12 (2006) 249–257.
[18] Y.C. Wong, Y.S. Szeto, W.H. Cheung, G. McKay, Effect of temperature, particle size and percentage deacetylation on the adsorption of acid dyes on chitosan, Adsorption 14 (2008) 11–20.
[19] M. Chiou, P. Ho, H. Li, Adsorption of anionic dyes in acid solutions using chemically cross-linked chitosan beads, Dyes Pigm. 60 (2004) 69–84.
[20] R.S. Juang, R.L. Tseng, F.C. Wu, S.H. Lee, Adsorption behavior of reactive dyes from aqueous solutions on chitosan, J. Chem. Technol. Biotechnol. 70 (1997) 391–399.
[21] M. Sugimoto, M. Morimoto, H. Sashiwa, H. Saimoto, Y. Shigemasa, Preparation and characterization of water-soluble chitin and chitosan derivatives, Carbohydr. Polym. 36 (1998) 49–59.
[22] F.H. Chi, W.P. Cheng, Use of chitosan as coagulant to treat wastewater from milk processing plant, J. Polym. Environ. 14 (2006) 411–417.
[23] H. Sashiwa, Y. Shigemasa, Chemical modification of chitin and chitosan 2: Preparation and water soluble property of N-acylated or N-alkylated partially deacetylated chitins, Carbohydr. Polym. 39 (1999) 127–138.
[24] N. Terada, M. Morimoto, H. Saimoto, Y. Okamoto, S. Minami, Y. Shigemasa, Synthesis of the aglycon of aurisides A and B, cytotoxic macrolide glycosides of marine origin. Chem. Lett. 28 (1999) 85–86.
[25] T.R. Sridhari, P.K. Dutta, Synthesis and characterization of maleilated chitosan for dye house effluent, Indian J. Chem. Technol. 7 (2000) 198–201.
[26] A. Heras, N.M. Rodriguez, V.M. Ramos, E. Agullo, N-methylene phosphonic chitosan: A novel soluble derivative, Carbohydr. Polym. 44 (2001) 1–8.
[27] Z. Liu, J. Ding, J. Xue, A new family of biocompatible and stable magnetic nanoparticles: Silica cross-linked pluronic F127 micelles loaded with iron oxides, New J. Chem. 33 (2009) 88–92.
[28] N. Shrestha, J. Macak, F. Schmidt-Stein, R. Hahn, C. Mierke, B. Fabry, P. Schmuki, Magnetically guided titania nanotubes for site-selective photocatalysis and drug release, Angew. Chem. Int. Ed. 48 (2009) 969–972.
[29] H. Deng, X.L. Li, Q. Peng, Monodisperse magnetic single-crystal ferrite microspheres, Angew. Chem. Int. Ed. 44 (2005) 2782–2785.
[30] S.Y. Chai, Y.S. Kim, W.I. Lee, Photocatalytic property of TiO_2 loaded with SnO_2 nanoparticles, J. Electroceram. 17 (2006) 323–326.
[31] Z.Y. Liu, H.W. Bai, D.D. Sun, Facile fabrication of porous chitosan/TiO_2/Fe_3O_4 microspheres with multifunction for water purifications, New J. Chem. 35 (2011) 137–140.
[32] M. Abdullah, G.K.C. Low, R.W. Matthews, Effects of common inorganic anions on rates of photocatalytic oxidation of organic carbon over illuminated titanium dioxide, J. Phys. Chem. 94 (1990) 6820–6825.